scientific reports

Check for updates

OPEN

Taletrectinib promotes pyroptosis in colorectal carcinoma via SRC/AKT/mTOR axis inhibition

Ting Zhang[1,3], Ye Zou[2,3], Sun-Han Zhang[2,3], Yuan-Yi Wang[2], Shuang He[2], Wei Yuan[2], Min Yang[1], Teng Liu[1], Shi-Hua Deng[1], Dong-Ming Wu[1] & Ying Xu[1]✉

Drug resistance develops frequently after colorectal carcinoma (CRC) surgery, indicating the urgent need for new therapeutic strategies. Taletrectinib (DS-6051b/AB-106), a synthetic ROS1/NTRK inhibitor which has shown meaningful antitumor activity, is currently undergoing clinical trials aimed at addressing targeted resistance. However, the anti-cancer effect of taletrectinib on CRC remains unclear. In this study, our purpose was to evaluate taletrectinib-related cytotoxicity in vitro using two CRC cell lines, as well as in vivo in a mouse tumor model. The mechanism underlying the cytotoxicity of taletrectinib was evaluated using light microscopy, scanning electron microscopy, immunofluorescence assays, an annexin V-FITC/propidium iodide detection, lactate dehydrogenase (LDH) release assays, and western blotting. We found that the viability of CRC cells decreased with increasing concentrations of taletrectinib. In addition, transcriptome sequencing indicated that HCT116 and LOVO cell lines did not carry ROS1- or NTRK-related gene fusions and that the cytotoxic effect of taletrectinib was exerted via caspase-3/gasdermin E (GSDME)-dependent pyroptosis. Moreover, the effect of taletrectinib in promoting pyroptosis was reversed by treatment with the SRC agonist, tolimidone, both in vitro and in vivo. Overall, our findings suggest that taletrectinib suppresses tumor growth by inducing GSDME-mediated pyroptosis via the SRC/AKT/mTOR signaling pathway, indicating that taletrectinib shows potential as a promising therapeutic agent against CRC.

Keywords Colorectal carcinoma, Taletrectinib, Pyroptosis, GSDME, SRC

Abbreviations

GSDME	Gasdermin E
CRC	Colorectal cancer
PI	Propidium iodide
LDH	Lactate dehydrogenase
SRC	Non-receptor tyrosine kinase c-SRC
PARP	Poly-ADP-ribose polymerase
CCK8	Cell counting kit-8 assay
DAPI	4',6-diamidino-2-phenylindole
TUNEL	TdT-mediated dUTP Nick End Labeling
7-AAD	7-aminoactinomycin D
Z-DEVD	Z-DEVD-fmk
ELISA	Enzyme-linked immunosorbent assay
PPI	Protein–protein interaction

Colorectal cancer (CRC) is among the most common malignant gastrointestinal cancers. The dietary habits of those inhabiting Western nations usually involve high-protein and high-fat foods, the negative aspects of which are compounded by a fast-paced urban lifestyle. The influence of foreign dietary concepts and lifestyles, has resulted in the incidence of CRC in China increasing annually since 1990[1]. The latest Global Cancer Statistics 2020 report, released by the World Health Organization, indicates that CRC ranks.

third in newly diagnosed cancer cases and second in cancer deaths globally[2]. Most patients with CRC are diagnosed at an advanced stage, and thus do not qualify for radical surgical treatment. Therefore, chemotherapy

[1]School of Clinical Medicine, The First Affiliated Hospital of Chengdu Medical College, Chengdu 610500, China. [2]School of Clinical Medicine, Chengdu Medical College, Chengdu, Sichuan, China. [3]Ting Zhang, Ye Zou and Sun-Han Zhang contributed equally to this work. ✉email: yingxu825@126.com

presents an important treatment option for patients with advanced CRC[3,4]. Accordingly, identifying new therapeutic drugs and elucidating their potential mechanisms of action may be considered as crucial.

Pyroptosis is a form of lytic cell death that primarily manifests as inflammation. In 2001, Cookson and Brennan proposed that pyroptosis is mediated by caspase-1[5]. Moreover, another form of programmed cell death caused by chemotherapeutic drugs, which is characterized by cell swelling and the emergence of large bubbles from the cell membrane, has been discovered[6]. Various studies have shown that pyroptosis is characterized by cellular dissolution. Moreover, it is reportedly triggered by the N-terminal domain of gasdermin E (GSDME), which is activated by the cleavage of caspase-3[7–9] and is also responsible for the proteolytic activation of poly ADP-ribose polymerase (PARP) during apoptosis[10,11]. These findings indicate that pyroptosis may play a vital role in chemotherapy.

With due consideration given to the above findings, we screened 441 compounds, obtained from the Pyroptosis Compound Library, for potential novel chemotherapeutic agents. As a result, we found that, taletrectinib exerts a promising killing effect on CRC cells. Taletrectinib is an orally administered, small-molecule tyrosine kinase inhibitor with high affinity and specificity for ROS1 or NTRK receptors[12,13]. Preclinical studies conducted using ROS1 and NTRK as targets have shown excellent activity in vitro, as well as in in vivo, as seen in animal models of human tumors carrying the *ROS1*/*NTRK* gene fusion[14]. However, the effects exerted by taletrectinib on tumors such as CRC, which lack this alteration, have not been reported, prompting us to explore other relevant mechanisms in CRC cells, which are known to lack the *ROS1*/*NTRK* gene fusion.

SRC is a non-receptor tyrosine kinase encoded by the proto-oncogene *Src*. Abnormal SRC activation has been observed in many human malignant tumors, including CRC[15]. SRC overexpression or overactivation is closely related to the development, maintenance, and progression of human cancer, suggesting that it is an important target for cancer treatment[16]. Furthermore, studies have shown that SRC comprises the hub of several signaling pathways, such as AKT/mTOR that control cell proliferation, survival, invasion, migration, and angiogenesis[17–20] Further, this protein is inhibited in tumors and can induce pyroptosis[21]. According to previous studies, SRC overexpression accounts for nearly 80% of CRC cases[22]. Therefore, drug-mediated inhibition of SRC may improve tumor treatment. In this study, we explored the therapeutic relationship between SRC and taletrectinib, as investigating such effects of drugs and the associated mechanisms may provide new ideas for effective disease treatment and prevention.

Results

Taletrectinib inhibits CRC cell survival but not by suppressing the ROS1/NTRK fusion gene

We performed a CCK8 assay on HCT116 cells, to screen small molecule drugs from the Pyroptosis Compound Library that were effective against CRC (Fig. 1A). Next, we selected 17 drugs with inhibition rates of more than 50% to act on HCT116 and LoVo cells at a concentration of 10 μM for 24 h to conduct a secondary screening of the drugs (Fig. 1B). Based on a comparison of inhibition rates of the two groups of cells, we selected 17 drugs according to their ability to inhibit tumor cells and identified five top-performing drugs, namely gambogic acid, fludarabine phosphate, taletrectinib, R-7050, and ganetespib. These five small molecules were screened again via a CCK8 assay of HCT116 and LoVo cells, and the results indicated that taletrectinib ($C_{29}H_{34}FN_5O_5$) showed the most potential as an anti-CRC compound (Fig. 1C). The structural formula of taletrectinib is shown (Fig. 1D).

Taletrectinib is an effective, orally active, next-generation selective ROS1/NTRK inhibitor that is effective against tumors harboring *ROS1*/*NTRK* fusions[12,13]. To the best of our knowledge, the incidence of *ROS1*/*NTRK* rearrangements is very low in CRC[23]. Therefore, we performed transcriptome sequencing to determine whether the effects exerted on the two CRC cell lines used in this study were related to *ROS1*/*NTRK* gene fusion. The results indicated that these cell lines did not carry *ROS1*- or *NTRK*-related gene fusions (Fig. 1E). Therefore, we speculated that taletrectinib may inhibit CRC cell viability via other mechanisms. We treated HCT116 and LoVo cells with different concentrations of taletrectinib (0, 1.25, 2.5, 5, 10, and 20 μM) for 24 h and then performed a CCK8 assay to screen for the optimal working concentration of the drug. The results showed that the viability of HCT116 and LoVo cells decreased significantly with increasing drug concentration (Fig. 1F), with 5 μM of taletrectinib reducing cell viability by approximately 50%. Therefore, this concentration was chosen for subsequent experiments.

Taletrectinib induces pyroptosis in CRC cells

The observed cytotoxic effects prompted us to further investigate the mechanism underlying cell death induced by taletrectinib. Remarkably, we observed that taletrectinib treatment of CRC cells induced cell swelling and the formation of large bubbles in the cytoplasmic membrane, which is similar to the morphological features of cell pyroptosis (Fig. 2A). When single cells were further observed under a scanning electron microscope, bubbling was observed on the porous cell surfaces (Fig. 2B). In addition, we performed a TUNEL assay to determine the effect of taletrectinib on CRC cells. TUNEL staining was used to detect DNA breakage in the cells, and the results showed that cell damage in the taletrectinib-treated group was greater than that in the control group; indicating that taletrectinib treatment promotes cell death in a significant manner (Fig. 2C).

Furthermore, annexin-V PE/7-AAD staining based flow cytometry was performed to detect the type of cell death induced by taletrectinib. During typical cell apoptosis, the cell status changes from the early stage (annexin-V PE^+/7-AAD^-) of apoptosis to the late stage (annexin-V PE^+/7-AAD^+) of pyroptosis. After taletrectinib treatment, CRC cells underwent cell pyroptosis, as shown by an increase in the number of annexin-V PE^+/7-AAD^+ cells (Fig. 2D). Correspondingly, the release of LDH from CRC cells increased following taletrectinib treatment, further confirming the rupture of the cell membrane and resulting leakage (Fig. 2E). Recently, many studies have reported that pyroptosis, which is triggered by caspase-3-mediated activation of the N-terminal domain of GSDME, may be associated with the proteolytic activation of PARP[8–10]. Western blotting showed that taletrectinib treatment had increased the levels of active-caspase-3 and the N-terminal fragment of GSDME, as

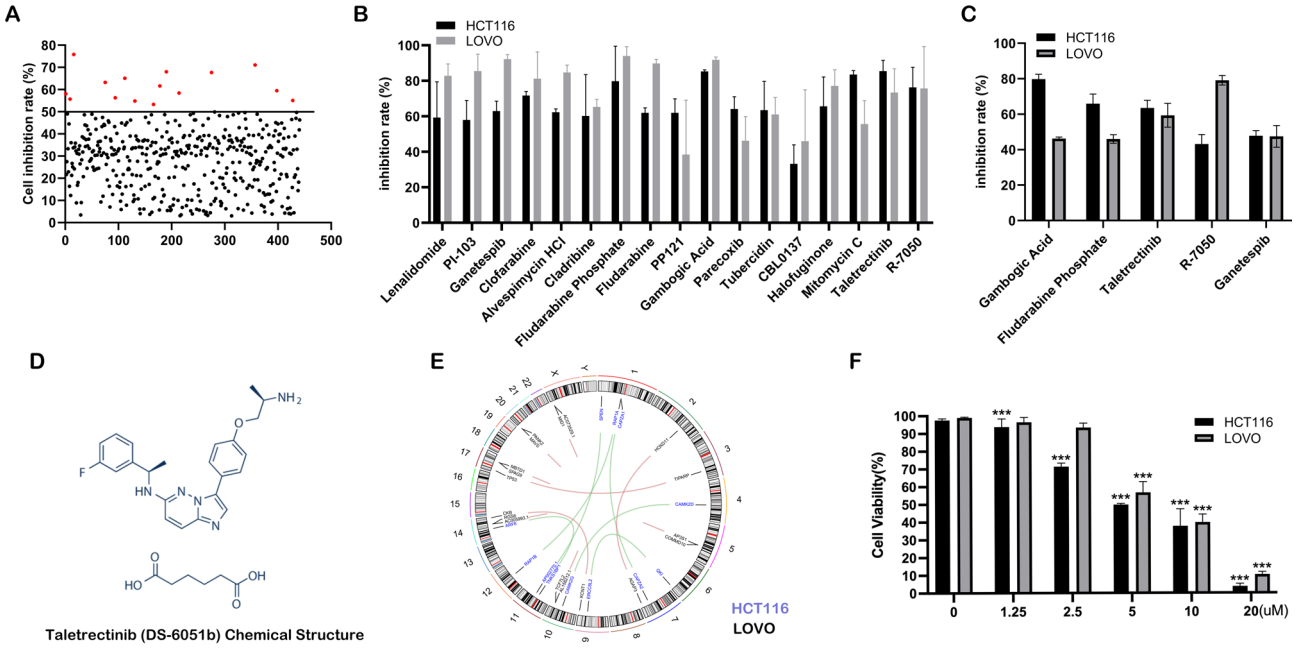

Fig. 1. Taletrectinib regulates colorectal cancer cell damage. (**A**) HCT116 cells treated with small molecule drugs from the Pyroptosis Compound Library, were subjected to a CCK8 assay to detect changes in the tumor cells inhibition rate. (**B**) CCK8 assay was used to determine the inhibition rate of HCT116 and LoVo cells treated with 17 selected drugs. (**C**) Five small molecules were used to treat CRC cells. CCK8 assay results showed that taletrectinib exerted the best effect on two types of cells. (**D**) Small molecule structure of taletrectinib. (**E**) Transcriptome sequencing of HCT116 and LoVo cells. A *ROS1*/*NTRK* fusion gene was not found in either cell line. (**F**) Results of the CCK-8 assay. HCT116 and LoVo cells were treated with taletrectinib at different concentrations for 24 h. *** $P < 0.001$.

well as the activation of PARP, in HCT116 and LoVo cells (Fig. 2F). This result is consistent with those of other studies[24–27].

Taletrectinib exerts cytotoxic effects through caspase-3/GSDME-dependent pyroptosis

To verify whether caspase-3/GSDME-dependent pyroptosis is involved in the cytotoxicity of taletrectinib, we treated CRC cells with the caspase-3 inhibitor, Z-DEVD. Morphologically, treatment with Z-DEVD significantly reduced the swelling and bubbles in the cell membrane induced by taletrectinib (Fig. 3A). Z-DEVD treatment also restored the viability of HCT116 and LoVo cells inhibited by taletrectinib (Fig. 3B). As expected, Z-DEVD treatment decreased the release of LDH induced by taletrectinib, indicating the suppression of cell membrane rupture and leakage (Fig. 3C). Moreover, western blotting indicated that Z-DEVD treatment had not only inhibited the activation of caspase-3 but also abrogated the activation of PARP and GSDME-N (Fig. 3D). To unequivocally validate the necessity of GSDME in taletrectinib-induced pyroptosis and rule out alternative apoptotic pathways, an shRNA lentiviral vector was used to stably knockdown GSDME in HCT116 and LoVo cells. As shown in Fig. 3E,F, the mRNA and protein levels of GSDME were reduced by at least 75% by H_GSDME-shRNA3. Therefore, we selected this shRNA for the subsequent experiments. Flow cytometry analysis revealed that taletrectinib-treated CRC cells exhibited a marked accumulation in the Annexin V+/7-AAD + quadrant, an effect that was substantially reversed upon GSDME knockdown (Fig. 3G). Consistent with these findings, LDH release assays demonstrated that GSDME knockdown significantly attenuated taletrectinib-induced LDH elevation (Fig. 3H). These results confirmed that the cytotoxic effect of taletrectinib in CRC cells is exerted via caspase-3/GSDME-dependent pyroptosis.

Taletrectinib targets SRC to inhibit AKT/mTOR signaling in CRC cells

We further explored the potential mechanism underlying caspase-3/GSDME-dependent pyroptosis induced by taletrectinib. The structure of taletrectinib was imported into the Swiss Target Prediction website, and 100 potential drug–protein targets were obtained. We reviewed the literature and selected 202 potential targets of taletrectinib with inhibitory concentrations greater than zero[28]. Based on intersection, 28 potential targets were identified. Subsequently, 161, 34, 196, and 1997 known therapeutic protein targets of CRC were obtained from the TTD, OMIM, DrugBank, and UniProt databases, respectively. Finally, 2388 known CRC targets were identified after eliminating redundancies. To obtain the anti-CRC target of taletrectinib, potential targets were cross-referenced with those having CRC listed as a treatment target. These criteria yielded 10 proteins (Fig. 4A). To identify the most critical anti-CRC target, a PPI (protein–protein interaction) network containing 10 interactive targets was constructed. Network topology was analyzed using the central algorithm, and the first

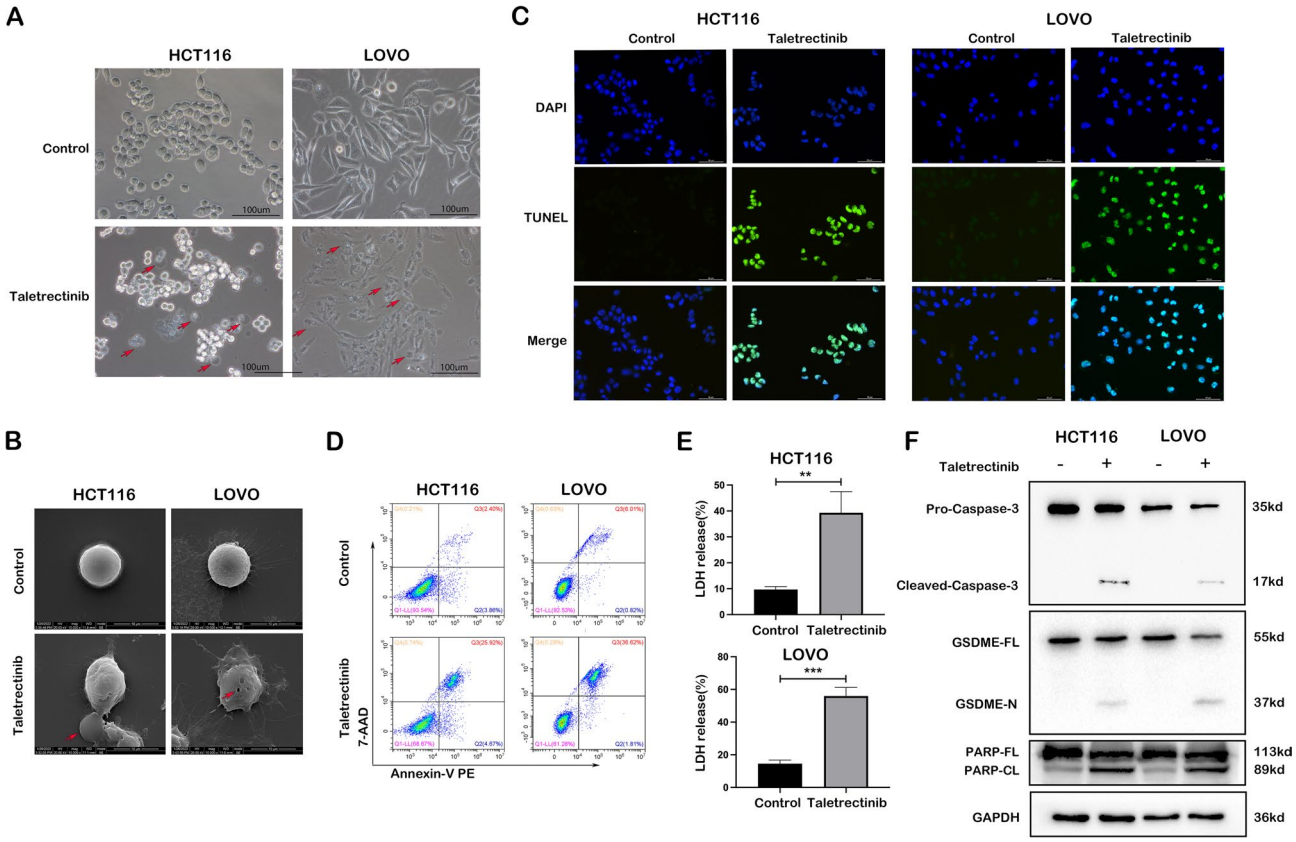

Fig. 2. Taletrectinib induces pyroptosis in colorectal cancer cell lines. HCT116 and LoVo colon cancer cells were treated with 5 μM taletrectinib for 24 h. (**A**) Large bubbles on the cell surface were observed under a microscope. (**B**) Large bubbles and pores appeared on the surface of single cells, as observed under a scanning electron microscope. (**C**) The number of dead cells increased after drug treatment, as observed via immunofluorescence. (**D**) Annexin V-PE/7-amino actinomycin D staining was used to detect pyroptosis in the HCT116 and LoVo cell lines. (**E**) A lactate dehydrogenase (LDH) release test was used to detect cytotoxicity following treatment with taletrectinib. (**F**) Western blotting was used to detect the protein expression of caspase-3, cleaved-caspase-3, gasdermin E (GSDME), GSDMDE-N, PARP, PARP-NL, and GAPDH in HCT116 and LoVo cells. $^{**}P < 0.01$, $^{***}P < 0.001$.

10 targets were summarized according to algorithm results (Fig. 4B). Based on the aforementioned confidence analysis, SRC was selected as the potential key target of taletrectinib.

Because the selected target SRC was a kinase, we first detected the change in SRC kinase activity in CRC cells before and after drug treatment using an ELISA. There was no significant change in SRC kinase activity in CRC cells before or after taletrectinib treatment (Fig. 4C). To determine the specific role of taletrectinib in regulating SRC, we examined the mRNA levels of SRC in different groups. The results showed no significant changes in SRC mRNA levels, suggesting that taletrectinib has a post-translational regulatory effect on SRC kinase (Fig. 4D). SRC regulates proliferation, migration, invasion, and metastasis of cancer cells, which are regulated by signaling pathways, such as AKT/mTOR[29,30]. Previous studies have shown that aberrant activation of SRC promotes tumor formation, including melanoma, pancreatic, lung, head, and neck tumors[31–34]. Furthermore, AKT/mTOR signaling is also apparently dysregulated in numerous human malignancies, resulting in a chemo-resistance phenotype[35,36]. Therefore, we speculated that SRC might be an upstream regulator of AKT/mTOR. Our results showed that the phosphorylation of AKT and mTOR was markedly inhibited by taletrectinib (Fig. 4E). Tolimidone has been used in the literature as an SRC activator, so we added Tolimidone to activate SRC activity[37]. In addition, when SRC agonist tolimidone was preincubated with CRC cells prior to taletrectinib application, tolimidone increased the protein expression level of SRC and reversed the inhibition of p-AKT and p-mTOR by taletrectinib (Fig. 4F).

Taletrectinib regulates GSDME-dependent pyroptosis by targeting the inhibition of SRC. We utilized the SRC agonist, tolimidone, in studies aimed at further exploring the role played by SRC in taletrectinib-mediated pyroptosis. Light microscopy results showed that pretreatment with tolimidone had ameliorated cell swelling and large bubble formation induced by taletrectinib in the cell membrane (Fig. 5A). The number of annexin-V $PE^+/7\text{-}AAD^+$ cells in H1650 and LoVo cells treated with tolimidone and taletrectinib was significantly decreased, compared to that in the taletrectinib treatment group (Fig. 5B). Moreover, the release of LDH induced by taletrectinib in H1650 and LoVo cells was also reversed by pretreatment with tolimidone (Fig. 5C). Similarly, western blotting showed that pretreatment with tolimidone had inhibited the increase in active-caspase-3,

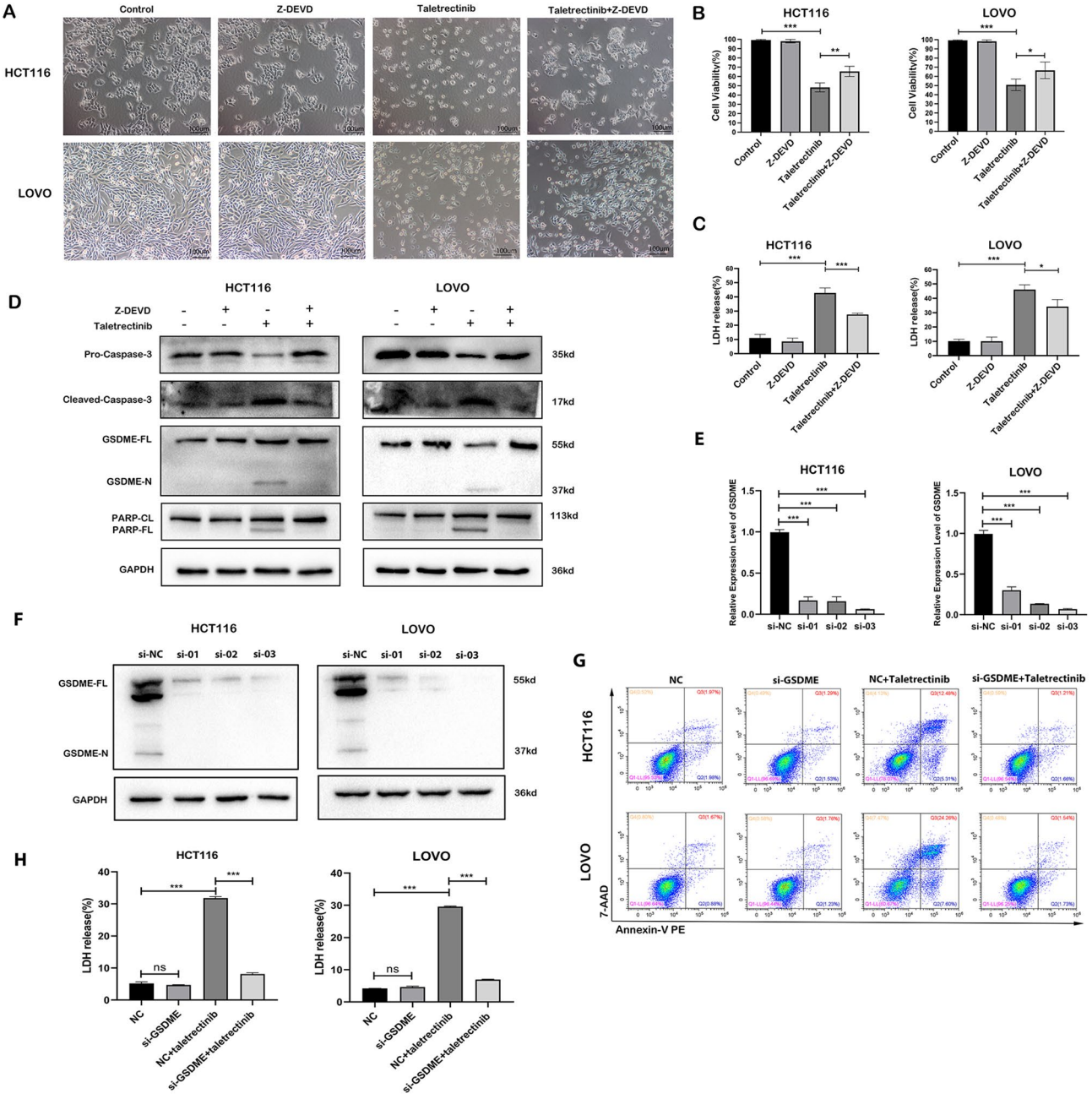

Fig. 3. Taletrectinib activates caspase-3/GSDME-mediated pyroptosis in colorectal cancer cell lines. HCT116 and LoVo cells were pretreated with Z-DEVD for 1 h and then treated with 5 μM taletrectinib for 24 h. (**A**) Microscopic images showing the morphological features of pyroptosis, including pyroptosis, of cells. (**B**) Changes in cell viability were detected using a cell counting kit-8 assay. Pretreatment with z-VAD significantly reversed the inhibitory effect of taletrectinib on colon cancer cell survival. (**C**) A lactate dehydrogenase (LDH) release test was used to detect the cytotoxic effects on cells. Pretreatment with Z-DEVD alleviated LDH release. (**D**) Western blotting was used to detect protein expression of caspase-3, cleaved-caspase-3, gasdermin E (GSDME), GSDME-N, PARP, PARP-NL, and GAPDH in HCT116 and LoVo cells. (**E**) RT-qPCR experiments to verify GSDME knockdown efficiency in HCT116 and LoVo cells. (**F**) Western blotting to verify GSDME knockdown efficiency in HCT116 and LoVo cells. (**G**) Flow cytometry was used to detect the proportion of Annexin V+/7-AAD + cells. (**H**) The LDH release assay is used to detect cytotoxic effects in different groups. $^{*}P < 0.05$, $^{**}P < 0.01$, $^{***}P < 0.001$.

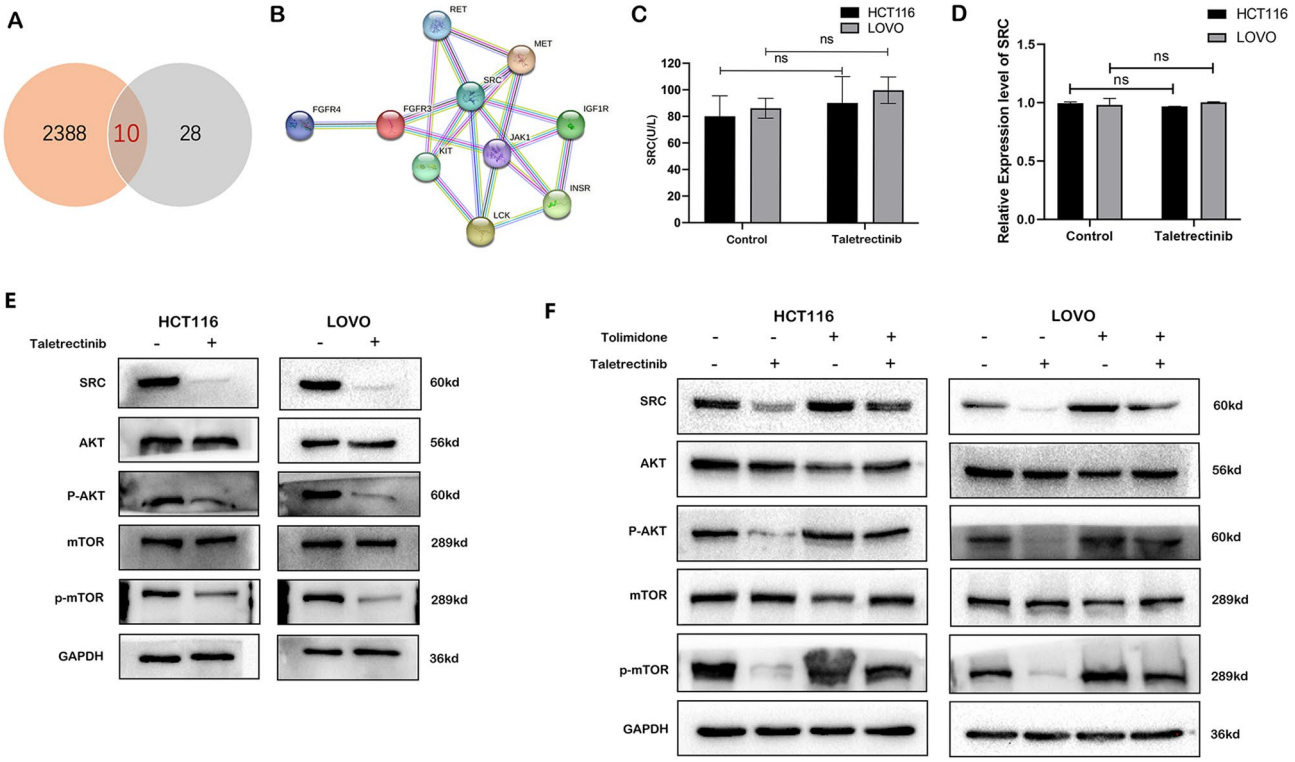

Fig. 4. Taletrectinib inhibits AKT/mTOR phosphorylation through SRC. (**A**) Venn diagram of taletrectinib and potential colon cancer treatment targets. (**B**) Diagram showing the protein interaction network. (**C**) Detection of SRC kinase activity upon treatment with taletrectinib, via ELISA. There was no significant difference in SRC activity after colon cancer cell treatment. (**D**) qPCR results show the expression levels of SRC in different groups. (**E**) Western blotting results showing the expression levels of SRC, AKT, mTOR, p-AKT, and p-mTOR proteins in HCT116 and LoVo cells treated with taletrectinib for 24 h. (**F**) SRC was ectopically expressed in colon cancer cells, and western blotting was used to detect SRC, AKT, mTOR, p-AKT, and p-mTOR protein expression levels in HCT116 and LoVo cells. ns, $P > 0.05$.

GSDME-N, and activated PARP, induced by taletrectinib treatment, in HCT116 and LoVo cells (Fig. 5D). Collectively, these results showed that the SRC agonist, tolimidone, had inhibited the effects of taletrectinib in promoting GSDME-dependent pyroptosis of CRC cells.

Taletrectinib exerts antitumor effects through GSDME-dependent pyroptosis in mice

Because our results indicated that taletrectinib may promote CRC cell death via GSDME-dependent pyroptosis by inhibiting the AKT/mTOR signaling pathway at the cellular level, we attempted to verify the antitumor effect of taletrectinib in vivo. We injected CRC cells subcutaneously into BALB/c-nude mice to successfully construct a mouse CRC xenograft model (Fig. 6A). Compared with those of the control group, the volume and weight of tumors were remarkably reduced following taletrectinib treatment; however, that effect was partially reversed by treatment with tolimidone (Fig. 6B–D). Furthermore, the decrease in the release of LDH and the inflammatory cytokines, IL18 and IL-1β, induced by taletrectinib, was partially offset by tolimidone (Fig. 6E–G). Moreover, an immunohistochemical analysis of tumor tissues indicated that taletrectinib had increased the expression levels of caspase-3 and GSDME-N, and decreased the expression levels of p-AKT and p-mTOR, thereby substantiating our previous findings (Fig. 6H). Thus, these results provided strong evidence that taletrectinib restrains tumor growth via GSDME-dependent pyroptosis.

Discussion

The annual incidence of CRC, one of the deadliest diseases of the gastrointestinal tract, is increasing among young people[2]. The prognosis for advanced CRC, which is very poor, exerts a negative impact on society as well as individuals[38]. Other than surgery, effective patient-specific treatments are currently lacking. Although significant progress has been made in the understanding of the pathogenesis of this disease, the availability of clinical treatments remains limited, leading to a poor quality of life for patients with CRC. Therefore, development of new drugs or treatment strategies for patients with CRC who are ineligible for surgical or advanced palliative treatments may be considered crucial[39].

Studies have indicated that pyroptosis contributes to tumor chemotherapy[9]. Another study reported that the combined treatment of olaparib and decitabine had synergistically induced pyroptosis and enhanced antitumor responses, ultimately alleviating tumor progression[40]. These results indicate that chemical drugs may inhibit the

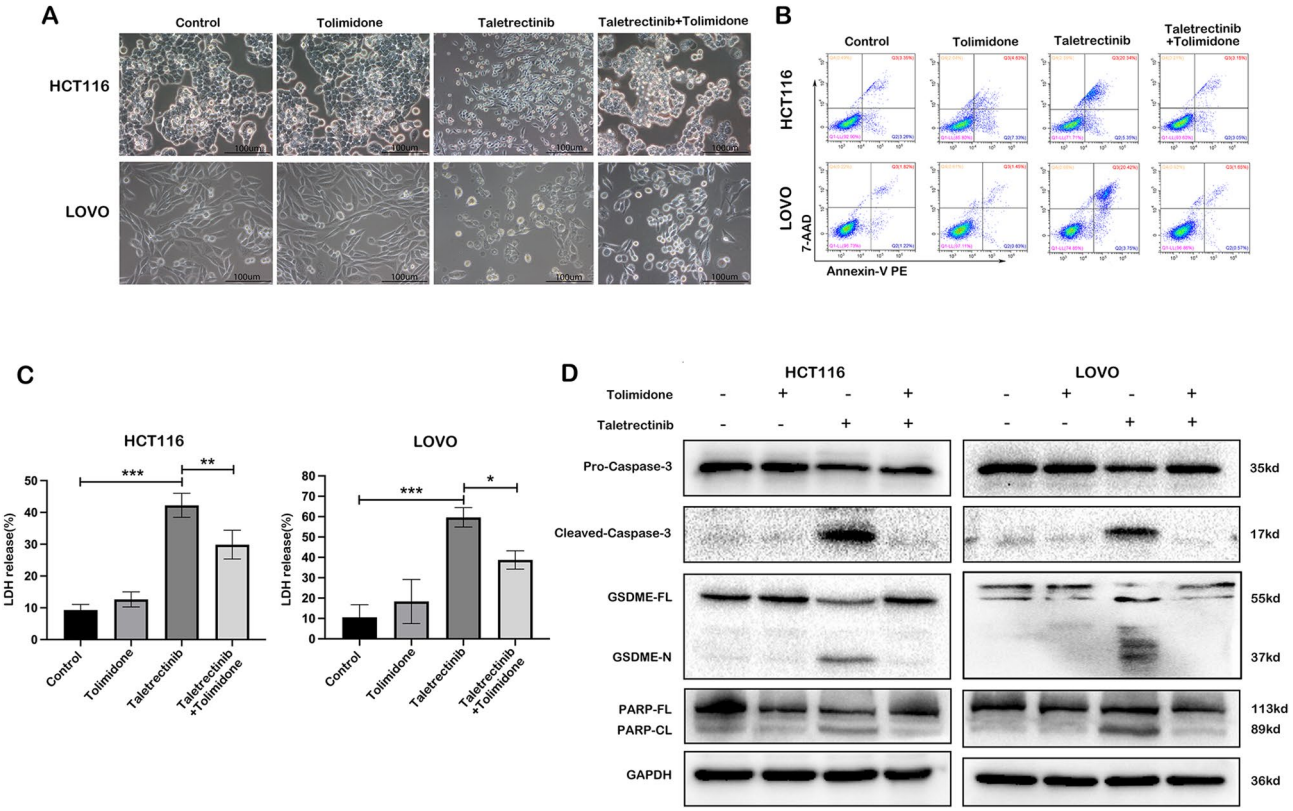

Fig. 5. Taletrectinib induces colorectal cancer cell pyroptosis by inhibiting SRC. SRC expression was upregulated through cell transfection, and taletrectinib treatment was performed for 24 h. (**A**) Microscopic images showing morphological changes, characteristic of pyroptosis, observed in cells. (**B**) Annexin V-PE/7-AAD staining was performed to determine the proportion of pyroptotic cells. (**C**) A lactate dehydrogenase (LDH) release cytotoxicity test showed that SRC overexpression may reduce LDH release caused by taletrectinib treatment. (**D**) Western blotting was performed to detect the protein expression of caspase-3, cleaved-caspase-3, gasdermin E (GSDME), GSDMDE-N, PARP, PARP-NL, and GAPDH in HCT116 and LoVo cells. $^{*}P < 0.05$, $^{**}P < 0.01$, $^{***}P < 0.001$.

growth of tumor cells by activating pyroptosis. The available data suggest that if the expression level of GSDME is low, caspase-3 activation mainly leads to apoptosis, and if GSDME is highly expressed, pyroptosis is favored[41]. When caspase-3 is activated, it cleaves GSDME to generate an N-terminal fragment with pore-forming activity, leading to cell membrane perforation, release of contents and inflammatory factors, and inflammatory responses characteristic of pyroptosis[25]. In this study, we screened drugs derived from the Pyroptosis Compound Library and finally selected taletrectinib for further analysis. As a small-molecule inhibitor, taletrectinib had already been tested in Phase I clinical trials. Taletrectinib is known to be a potent and selective ROS1/NTRK kinase inhibitor[12,13]. However, its effects on CRC cells have remained unclear. In this study, we found that taletrectinib effectively inhibits the proliferation of CRC cells and triggers cell death. We further studied the potential pyroptotic mechanism underlying the effects exerted by taletrectinib on CRC cells. We found that the CRC cell lines showed unique pyroptotic characteristics following taletrectinib treatment. These pyroptotic characteristics were associated with caspase-3 activation and GSDME cleavage. Importantly, we found that pretreatment with the caspase-3 inhibitor, Z-DEVD, blocks all aforementioned pyroptosis-related characteristics. Considered together, we found that caspase-3/GSDME-dependent cell death is associated with taletrectinib-treated CRC cell destruction, which is consistent with previous reports indicating that tumor cell pyroptosis may be induced by chemotherapeutic drugs[39].

Previous studies have shown that taletrectinib, a ROS1/NTRK inhibitor, is most effective against non-small cell lung cancer, which has a high incidence of ROS1/NTRK rearrangements. However, the incidence of ROS1/NTRK rearrangements in CRC is as low as 0.5–2.4%[23]. In this study, we found that taletrectinib also exerts a good killing effect on CRC cells without ROS1/NTRK rearrangements, and that its specific mechanism does not involve the inhibition of ROS1 or NTRK. Therefore, we explored alternate targets. Having established intersection in databases via cross-alignment, we conducted a comprehensive analysis which revealed that SRC may be a potential target of taletrectinib. SRC, which is highly expressed in CRC, regulates cell proliferation, differentiation, and adhesion. It also regulates cell proliferation and adhesion via the phosphorylation of AKT/

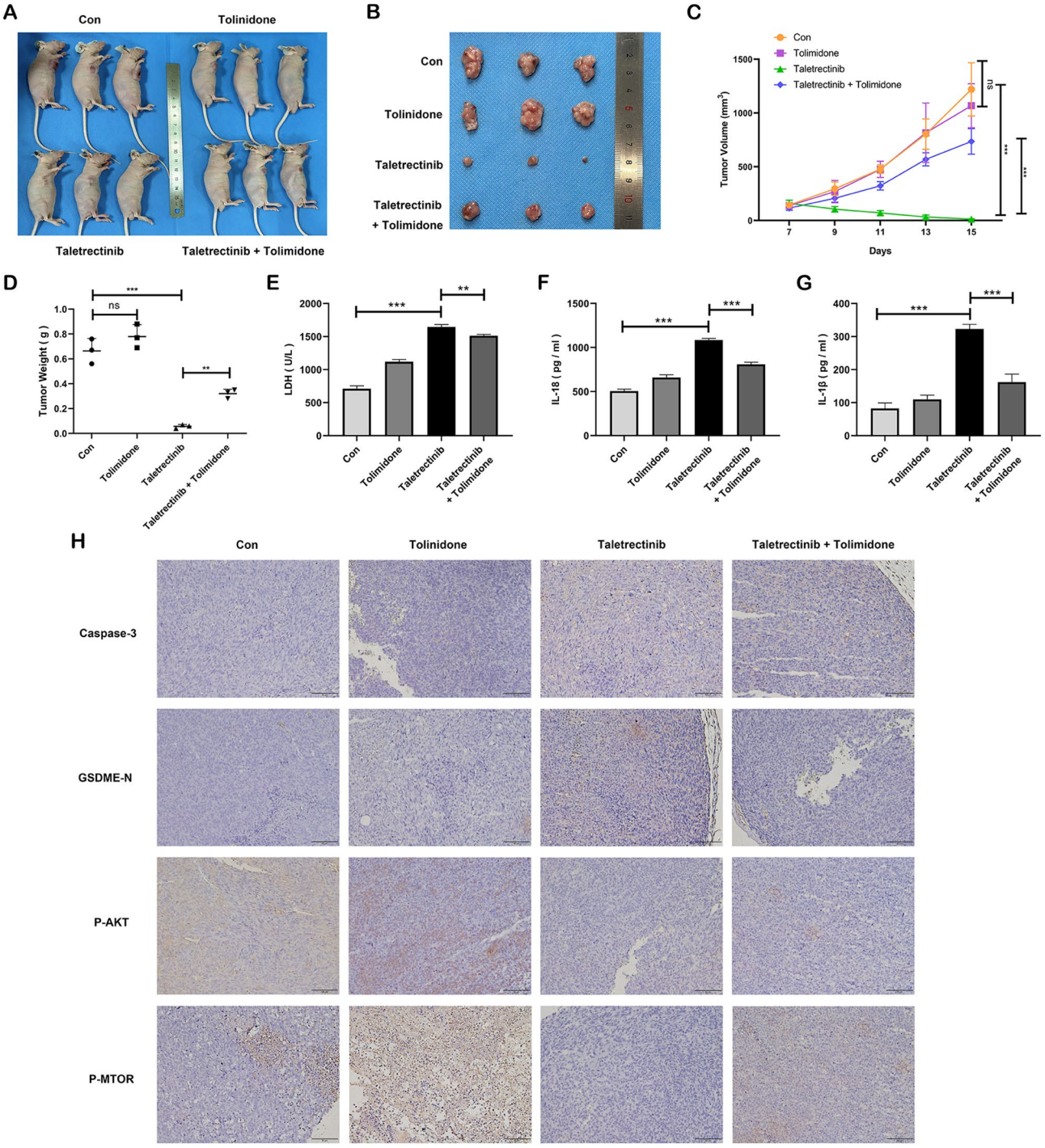

Fig. 6. Taletrectinib exerts antitumor effects through GSDME-dependent pyroptosis in mice. (**A**) Overall images of subcutaneous xenografts in nude mice in each group. (**B**) Xenograft tumors were isolated from sacrificed mice (14 days) following PBS, taletrectinib (50 mg/kg every other day), or tolimidone (30 mg/kg every other day) treatment. (**C**) Kinetics of tumor growth by volume of subcutaneous xenograft tumors. (**D**) Average weights of xenograft tumors in each group. (**E–G**) Release of serum LDH and secretion of IL-18 and IL-1β in nude mice. (**H**) Immunohistochemistry of caspase-3, GSDME-N, p-AKT, and p-mTOR in subcutaneous mouse tumors from the control, taletrectinib, taletrectinib + tolimidone, and tolimidone groups (scale bar, 100 μm). $^{**}P < 0.01$, $^{***}P < 0.001$.

mTOR pathway components[17]. Some studies have also shown that SRC inhibition, mediated by drugs, can lead to cell damage, thereby causing tumor pyroptosis[26]. According to previous reports, SRC is highly expressed in a variety of tumors, including CRC, with expression rates as high as 80% in some cancers[22]. In this study, we found that taletrectinib affected CRC cells via SRC, as specifically indicated by the phosphorylation of SRC,

AKT, and mTOR being significantly inhibited in CRC cells treated with taletrectinib. However, when SRC was overexpressed in these cells, taletrectinib-mediated SRC inhibition was significantly alleviated, the inhibition of AKT/mTOR phosphorylation was reversed, and pyroptosis characteristics were suppressed. Therefore, these observations suggested that taletrectinib promotes cell death by inhibiting SRC expression.

Finally, in order to demonstrate the inhibitory effects exerted by taletrectinib on the proliferation of CRC in vivo, we established a mouse subcutaneous xenograft tumor model and showed that taletrectinib can significantly reduce the weight and volume of tumors. In addition, immunohistochemical results of tumor tissues indicated that taletrectinib had increased the expression of caspase-3 and GSDME and inhibited the expression of p-AKT and p-mTOR to promote pyroptosis and CRC cell death. Thus, taletrectinib, a new SRC inhibitor, which causes caspase-3/GSDME-mediated cell death, shows potential as a prospective therapeutic option for CRC. Although we showed that the mechanism via which taletrectinib targets CRC involves the inhibition of SRC protein expression, no in-depth studies indicating the manner in which the drug specifically acts on SRC proteins have been conducted Therefore, such limitations pertaining to this study may warrant further investigation.

Conclusion

In this study, we demonstrated that taletrectinib regulates CRC progression by mediating caspase-3/GSDME-dependent pyroptosis, both in vivo and in vitro. Notably, taletrectinib promotes pyroptosis by targeting SRC via the AKT/mTOR signaling pathway, ultimately suppressing CRC (Fig. 7). In summary, our findings indicate that taletrectinib shows potential as a therapeutic agent against CRC.

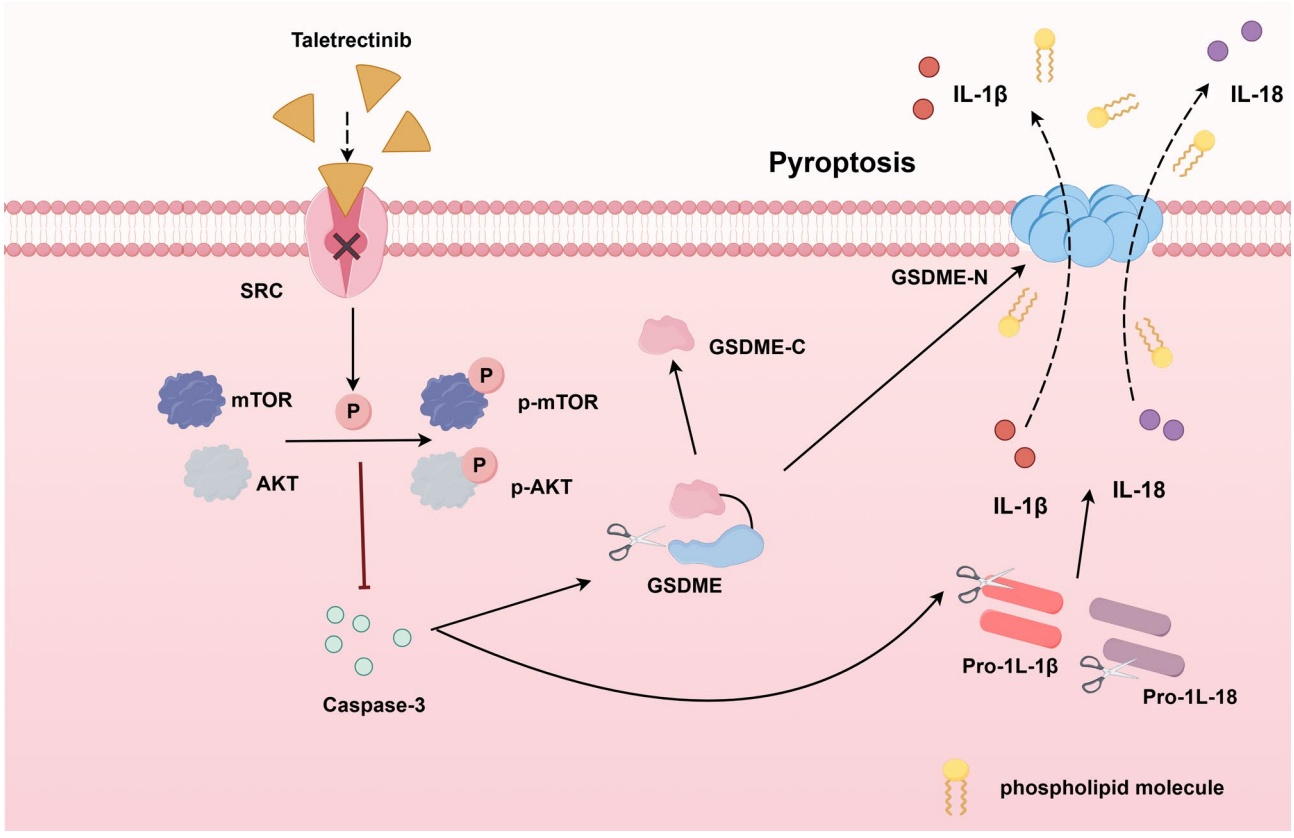

Fig. 7. Schematic summary of the proposed mechanism and function of taletrectinib in colorectal carcinoma. Taletrectinib inhibited the phosphorylation of AKT and mTOR by targeting SRC, induced caspase-3 activation, which contributed to GSDME-dependent pyroptosis, ultimately leading to CRC cells death.

Materials and methods

Cell culture

Human CRC cells (HCT116 and LoVo cells, purchased from Purcell, Wuhan, China) were cultured in RPMI-1640 (Cyclone, Hudson, NH, USA) culture medium supplemented with 200 U/mL penicillin G, 200 mg/mL

streptomycin, and 10% fetal bovine serum in a 5% CO_2 incubator at 37 °C. The cells were cultured until they reached 95% confluence for subsequent experiments.

Cell counting kit-8 (CCK8) assay

The Pyroptosis Compound Library was purchased from Selleck Chemicals (Houston, TX, USA), and its 441 compounds were stored as 10 mM stock solutions in dimethyl sulfoxide at 4 °C until needed. The viability of cells treated with 10 μM of every compound from this library for 24 h was measured using a CCK8 assay kit (Shanghai, China). HCT116 and LoVo cells were evenly inoculated into 96-well plates at a density of 4000 cells per well and incubated for 24 h. After the cells entered the logarithmic growth period, the original culture medium was discarded, and 100 μL of the medium was added. Different concentrations (0, 1.25, 2.5, 5, 10, and 20 μM) of taletrectinib were used to treat the cells. In other experiments, the effects of treatment with taletrectinib (5 μM) were evaluated at different time points with or without the Z-DEVD. Finally, 10 μL of the CCK8 solution was added to each well, and the cells were incubated at 37 °C for 1 h.

Transcriptome sequencing

HCT116 and LoVo cells in the logarithmic growth phase were inoculated into 10 cm-diameter cell culture dishes. When cell confluency exceeded 80%, the cells were rinsed with phosphate-buffered saline (PBS; Solarbio, Beijing, China) once or twice, and the PBS solution was completely removed. Next, cell scrapers were used to gently scrape the cells (not scraping them repeatedly), which were then collected in 1.5 mL tubes. Next, the cells were centrifuged at 1000 × g for 5 min and stored at − 80 °C. Finally, the samples were sent to SinoTech Genomics, Ltd. (Shanghai, China) for inspection.

Observation of cell morphology under a microscope

HCT116 and LoVo CRC cells were inoculated into 6-well plates and incubated. After the cells adhered to the plate, they were treated with drugs and cultured for 24 h. The cells were then observed under a microscope (500×, LEICA, Germany), and photographed.

TUNEL (TdT-mediated dUTP Nick End Labeling) experiment

HCT116 and LoVo CRC cells in the logarithmic growth phase were seeded in 24-well plates (1×10^5 cells/well). Following treatment with 5 μM taletrectinib, the cells were cultured for 24 h. The medium was then discarded, and the cells were washed twice with PBS. Then, 50 μL of TUNEL test solution was added to each well and incubated in the dark at 37 °C for 60 min. Next, the samples were washed thrice with PBS for 3 min each. Then, DAPI (4',6-diamidino-2-phenylindole) was prepared at a ratio of 1:10000, and the cells were incubated with this reagent at 37 °C in the dark for 5 min. Next, the samples were washed thrice with PBS (5 min each time). Finally, the slide was covered with a cover slip, and each plate was treated with 1 μM anti-fluorescence quenching agent (Beyotime, Shanghai, China), and examined under a microscopic.

Scanning electron microscopy

HCT116 and LoVo cells in the logarithmic growth phase were seeded in 24-well plates (1×10^5 cells/well) and incubated for 24 h. Cells were divided into control and drug-treated groups. The cells in the control group were treated with culture medium, whereas the HCT116 and LoVo cells in the drug group were treated with 5 μM taletrectinib for 24 h. Cells were washed thrice with PBS, the medium was removed, and the cells were stored at 4 °C with 2.5% (v/v) glutaraldehyde fixative (pH 7.3–7.4).

Flow cytometry

HCT116 and LoVo CRC cells were digested with 0.25% Trypsin (Invitrogen; Thermo Fisher Scientific, Inc.), washed and collected. We stained cells for 15 min with Annexin V-PE/7-AAD Apoptosis Detection Kit (Nanjing KeyGen Biotech Co., Ltd.) in the dark at room temperature according to the instructions. Cells were washed twice with PBS, and analyzed via flow cytometry (FACSCalibur, Becton–Dickinson, Franklin Lakes, NJ, USA).

Total RNA extraction and RT-qPCR

Total RNA was extracted from cells using the Total RNA Extraction Kit (Beijing Solarbio Science & Technology Co., Ltd.) under ice-cold conditions according to the manufacturer's protocol. RNA samples were reverse-transcribed into cDNA using the iScript cDNA Synthesis Kit (Bio-Rad Laboratories, Inc.). cDNA templates were combined with SYBR Green Supermix (Bio-Rad Laboratories, Inc.) and gene-specific primers on ice, followed by amplification on a CFX96 Real-Time PCR Detection System (Bio-Rad Laboratories, Inc.) under the following conditions: initial denaturation at 95 °C for 2 min, 40 cycles of 95 °C for 10 s, 62 °C for 30 s, and 72 °C for 30 s. Primer sequences were as follows: GSDME: Forward 5′-ATGTTTGCCAAAGCAACCAGGA-3′, Reverse 5′-TC ATGAATGTTCTCTGCCTAAAGCACA-3′; β-actin: Forward 5′-GGGCCGGACTCGTCATAC-3′, Reverse 5′-CCTGGCACCCAGCACAAT-3′.

GSDME knockdown

To achieve GSDME knockdown, three short hairpin RNAs (shRNAs) targeting distinct coding sequences of GSDME were designed and cloned into the pGMLV-SC5 RNAi lentiviral vector (Genomeditech, Shanghai, China) for lentiviral packaging and subsequent cell transduction. The shRNA target sequences were as follows: Negative control (NC): 5′-TTCTCCGAACGTGTCACGT-3′; shGSDME-1: 5′-GATGATGGAGTATCTGATC TT-3′; shGSDME-2: 5′-GGATTGTGCAGCGCTTGTTTG-3′; shGSDME-3: 5′-GCTTTAGGCAGAGAACAT TCA-3′. Lentivirus production and stable cell line generation were performed by Genomeditech. Knockdown efficiency was validated at both transcriptional and protein levels using RT-qPCR and Western blot analysis,

respectively, confirming significant reduction of GSDME expression in shRNA-transduced cells compared to the NC group.

Nude mouse subcutaneous tumor model

All xenograft experiments were performed following the guidelines of the Laboratory Animal Ethical Committee of Chengdu Medical College. All experimental protocols were approved by the Laboratory Animal Ethical Committee at Chengdu Medical College. A mouse subcutaneous xenograft CRC model was established to explore the therapeutic potential of taletrectinib on CRC in vivo. Male BALB/C-nude mice (4–5 weeks of age, 14–16 g) were purchased from Gempharmatech Co., Ltd. (Chengdu, China). Before conducting the experiments, the mice were randomly assigned to four treatment groups of three mice each: normal control (NC), taletrectinib, taletrectinib + tolimidone, and tolimidone. CRC cells (1×10^6) were suspended in 100 µL of serum-free RPMI-1640 medium and injected subcutaneously into the axilla of nude mice. Seven days after cell implantation, when the tumor volume was approximately 30–40 mm^3, the mice in each group were intraperitoneally injected with 100 µL of PBS, taletrectinib (50 mg/kg every other day), or tolimidone (30 mg/kg every other day). Tumor growth (V) was measured using vernier calipers, and tumor volume was determined using the formula: $V = (a \times b^2)/2$, where a and b are the maximum and minimum diameters, respectively, in millimeters. After 2 weeks, mice were deeply anesthetized with a single intraperitoneal injection of sodium pentobarbital (50 mg/kg body weight) for at least 10 min, followed by cervical dislocations to ensure humane euthanasia. Sodium pentobarbital (WKQ-0028128) was obtained from Vicky Biotechnology (Chengdu, China).

Lactate dehydrogenase (LDH) assay

The sera of dissected mice were collected, and the supernatant was centrifuged and the release of LDH was determined according to the instructions of the LDH assay kit (Nanjing Jiancheng Bioengineering Institute).

Inflammatory cytokine release assay

Collected mouse sera were centrifuged, the supernatant was obtained, and the levels of IL-8 and IL-1β were determined using an enzyme-linked Immunosorbent assay kit, according to the manufacturer's instructions (Shanghai, China).

Immunohistochemistry (IHC)

IHC was performed using a universal two-step detection kit (mouse/rabbit enhanced polymer detection system; cat. no. PV9000; ZSGB-BIO; OriGene Technologies, Inc.). The paraffin sections were dewaxed, dehydrated in fresh xylene and graded alcohol, and washed with PBS buffer. Next, the prepared sections were boiled in citric acid buffer (pH 6.0) under high pressure for target antigen retrieval. An appropriate amount of endogenous peroxidase blocker was added to the sections, incubated for 10 min at room temperature, and rinsed with PBS buffer. The sections were incubated at 4˚C overnight with primary antibodies, including anti-caspase-3 (1:200; cat. no. 19677-1-AP), anti-GSDME (1:200; cat. no. 13075-1-AP), anti-p-AKT (1:200; cat. no. 66444-1-Ig), anti-p-mTOR (1:1000; cat. no. 67778-1-Ig), all from Proteintech Group, Inc. After several rinses with PBS buffer, the sections were incubated with an appropriate amount of reaction enhancement solution at room temperature for 20 min. After multiple rinses using PBS buffer, the sections were incubated with an appropriate amount of enhanced enzyme labeled goat anti-mouse/rabbit IgG polymer, added dropwise, for 20 min at room temperature. Finally, the sections were rinsed with PBS buffer several times and then stained using a 3,3'-diaminobenzene (DAB) chromogenic kit (cat. no. ZLI-9017; ZSGB-BIO; OriGene Technologies, Inc.). Briefly, DAB was used as the chromogen to stain the reaction products for 3 min at room temperature for visualization. The sections were then counterstained with hematoxylin (Beyotime Institute of Biotechnology) at room temperature for 1 min. Random images were obtained at a magnification of 20× using a fluorescence microscope (IX71; Olympus Corporation).

Western blotting

HCT116 and LoVo CRC cells were treated with 5 µM taletrectinib and incubated for 24 h. Before that, Z-DEVD pre-treatment was performed or SRC overexpression was induced in CRC cells according to experimental requirements. Cells were lysed in RIPA buffer (Beyotime, Shanghai, China), and protein extracts (50 µg) were loaded onto the blots according to experimental requirements. SDS-PAGE was performed using an electrophoresis apparatus at 80 V, which was increased to 120 V after 30 min. The proteins were then transferred onto a PVDF membrane (Millipore, Billerica, MA, USA) at a constant current of 250 mA for 90 min. The samples were then shaken in TBS-T containing 5% (w/v) powdered skim milk (Ely, Nei Monggol, China) for 1 h and then incubated with the following antibodies: anti-caspase-3 antibody (1:1000; Wuhan Proteintech, China), anti-pro-caspase-3 (1:1000; Wuhan Proteintech, China), anti-cleaved caspase-3 (1:1000; Abcam, United States), anti-GSDME (1:1000; Abcam, United States), anti-PARP (1:1000; Wuhan Proteintech, China), and anti-GAPDH (1:5000; Wuhan Proteintech, China) at 4 °C. Next, samples were washed thrice with TBS-T (10 min each time) and incubated with goat anti-rabbit IgG/HRP and goat anti-mouse IgG/HRP (both 1:10000; Wuhan Proteintech, China) secondary antibodies at room temperature (27 °C) for 1 h.

SRC enzyme-linked immunosorbent assay (ELISA)

HCT116 and LoVo cells in the logarithmic growth phase were inoculated into 10 cm-diameter cell culture dishes. When cell density exceeded 50%, the cells were treated with 5 µM taletrectinib for 24 h. Next, we measured SRC activity using a SRC ELISA Kit (Jing, Shanghai, China), according to the manufacturer's instructions.

Statistical analysis

Data were analyzed using the GraphPad Prism 8.0 statistical program (GraphPad Software, San Diego, CA, USA). The Shapiro-Wilk normality test was used to determine whether the experimental data were normally distributed. The results of normally distributed data were presented as the mean ± standard error, and a two-tailed Student's independent sample t-test was used to compare two-groups, while One-way ANOVA was used to compare more than two normally distributed groups. For data that did not meet the normality assumption, the Kruskal Wallis test was used to determine statistical differences between three or more independent groups, and the Bonferroni correction was used for post hoc multiple comparisons. Each in vitro experiment was independently performed at least three times. Statistical significance was set at $P < 0.05$.

Data availability

Data supporting the findings of this study are available from the corresponding author upon request.

Received: 13 November 2024; Accepted: 16 May 2025
Published online: 24 May 2025

References

1. Gaines, S. et al. Western diet promotes intestinal colonization by collagenolytic microbes and promotes tumor formation after colorectal surgery. *Gastroenterology* **158**(4), 958–970. https://doi.org/10.1053/j.gastro.2019.10.020 (2020) (**PMC Free article**).
2. Sung, H. et al. Global cancer statistics 2020: GLOBOCAN estimates of incidence and mortality worldwide for 36 cancers in 185 countries. *CA Cancer J. Clin.* **71**(3), 209–249. https://doi.org/10.3322/caac.21660 (2021) (**PMC Free article**).
3. Chan, A., Woods, R., Kennecke, H. & Gill, S. Factors associated with delayed time to adjuvant chemotherapy in stage III colon cancer. *Curr. Oncol.* **21**(4), 181–186. https://doi.org/10.3747/co.21.1963 (2014).
4. Suto, T. *et al.* Preplanned safety analysis of the JFMC37-0801 trial: A randomized phase III study of six months versus twelve months of capecitabine as adjuvant chemotherapy for stage III colon cancer, *Int J Clin Oncol* 22(3) 494–504, (PMC Free article). https://doi.org/10.1007/s10147-016-1083-9, PubMed, Google Scholar [published correction appears in Int J Clin Oncol 2017 22(4):805–806. (2017). https://doi.org/10.1007/s10147-017-1146-6. doi: 10.1007/s10147-017-1146-6].
5. Cookson, B. T. & Brennan, M. A. Pro-inflammatory programmed cell death. *Trends Microbiol.* **9**(3), 113–114. https://doi.org/10.1016/s0966-842x (2001) (**PMC Free article**).
6. Jorgensen, I. & Miao, E. A. Pyroptotic cell death defends against intracellular pathogens. *Immunol. Rev.* **265**(1), 130–142. https://doi.org/10.1111/imr.12287 (2015) (**PMC Free article**).
7. Van Laer, L. et al. Nonsyndromic hearing impairment is associated with a mutation in DFNA5. *Nat. Genet.* **20** (2), 194–197. https://doi.org/10.1038/2503 (1998).
8. Rogers, C. et al. Cleavage of DFNA5 by caspase-3 during apoptosis mediates progression to secondary necrotic/pyroptotic cell death. *Nat. Commun.* **8**, 14128. https://doi.org/10.1038/ncomms14128 (2017).
9. Wang, Y. et al. Chemotherapy drugs induce pyroptosis through caspase-3 cleavage of a gasdermin. *Nature* **547**(7661), 99–103. https://doi.org/10.1038/nature22393 (2017) (**PMC Free article**).
10. Zhang, Z. et al. Gasdermin E suppresses tumour growth by activating anti-tumour immunity. *Nature* **579**(7799), 415–420. https://doi.org/10.1038/s41586-020 (2020) (**PMC Free article**).
11. Zhou, L. et al. Lead acetate induces apoptosis in Leydig cells by activating PPARγ/caspase-3/PARP pathway. *Int. J. Environ. Health Res.* **31**(1), 34–44. https://doi.org/10.1080/09603123.2019.1625034 (2021) (**PMC Free article**).
12. Ye, Y. et al. High-resolution mass spectrometry-based approach for the identification and profiling of the metabolites of Taletrectinib formed in liver microsomes. *Drug Test. Anal.* **13**(6), 1118–1126. https://doi.org/10.1002/dta.3008 (2021) (**PMC Free article**).
13. Papadopoulos, K. P. et al. U.S. Phase I first-in-human study of Taletrectinib (DS-6051b/AB-106), a ROS1/TRK inhibitor, in patients with advanced solid tumors. *Clin. Cancer Res.* **26**(18), 4785–4794. https://doi.org/10.1158/1078-0432 (2020) (**PMC Free article**).
14. Lara, P. C., Macías-Verde, D. & Burgos-Burgos, J. Age-induced NLRP3 inflammasome over-activation increases lethality of SARS-CoV-2 pneumonia in elderly patients. *Aging Dis.* **11**(4), 756–762 (2020) (**PMC Free article**).
15. Zhu, S. W. et al. pH-responsive nanoprodrugs combining a Src inhibitor and chemotherapy to potentiate antitumor immunity via pyroptosis in head and neck cancer. *Acta Biomater.* **154**, 497–509. https://doi.org/10.1016/j.actbio.2022.10.051 (2022) (**PMC Free article**).
16. Roskoski, R. Jr. Src protein-tyrosine kinase structure and regulation. Biochem. Biophys. *Res. Commun.* **324**(4), 1155–1164. https://doi.org/10.1016/j.bbrc.2004.09 (2004) (**PMC Free article**).
17. Li, J. et al. NCAM regulates the proliferation, apoptosis, autophagy, EMT, and migration of human melanoma cells via the Src/Akt/mTOR/cofilin signaling pathway. *J. Cell. Biochem* **121**(2), 1192–1204. https://doi.org/10.1002/jcb.29353 (2020).
18. Xia, P. & Xu, X. Y. PI3K/Akt/mTOR signaling pathway in cancer stem cells: from basic research to clinical application. *Am. J. Cancer Res.* **5**(5), 1602–1609 (2015).
19. Levin, V. A. Basis and importance of Src as a target in cancer. *Cancer Treat. Res.* **119**, 89–119. https://doi.org/10.1007/1-4020-7847 (2004) (**PMC Free article**).
20. Liu, Q. et al. Anesthetic propofol promotes tumor metastasis in lungs via GABAA R-dependent TRIM21 modulation of Src expression. *Adv Sci. (Weinh)* **8**(18), e2102079. https://doi.org/10.1002/advs.202102079 (2021) (**PMC Free article**).
21. Cho, Y. J., Lee, J. E., Park, M. J., O'Malley, B. W. & Han, S. J. Bufalin suppresses endometriosis progression by inducing pyroptosis and apoptosis. *J. Endocrinol.* **237**(3), 255–269. https://doi.org/10.1530/JOE-17-0700 (2018) (**PMC Free article**).
22. Chen, J., Elfiky, A., Han, M., Chen, C. & Saif, M. W. The role of Src in colon cancer and its therapeutic implications. *Clin. Colorectal Cancer* **13**(1), 5–13. https://doi.org/10.1016/j.clcc.2013.10.003 (2014) (**PMC Free article**).
23. Pietrantonio, F. et al. ROS1, and NTRK rearrangements in metastatic colorectal cancer. *J. Natl. Cancer Inst.* **109**(12), 10. https://doi.org/10.1093/jnci/djx089 (2017).
24. Yu, J. et al. Cleavage of GSDME by caspase-3 determines lobaplatin-induced pyroptosis in colon cancer cells. *Cell. Death Dis.* **10**(3), 193. https://doi.org/10.1038/s41419-019-1441-4 (2019) (**PMC Free article**).
25. Cheng, J. et al. A novel DFNA5 mutation, IVS8 + 4 A > G, in the splice donor site of intron 8 causes late-onset non-syndromic hearing loss in a Chinese family. *Clin. Genet.* **72**(5), 471–477. https://doi.org/10.1111/j.1399-0004.2007.00889 (2007) (**PMC Free article**).
26. Lage, H., Helmbach, H., Grottke, C., Dietel, M. & Schadendorf, D. DFNA5 (ICERE-1) contributes to acquired Etoposide resistance in melanoma cells. *FEBS Lett.* **494**(1–2), 54–59. https://doi.org/10.1016/s0014-5793 (2001) (**PMC Free article**).
27. Masuda, Y. et al. The potential role of DFNA5, a hearing impairment gene, in p53-mediated cellular response to DNA damage. *J Hum. Genet.* **51**(8), 652–664. https://doi.org/10.1007/s10038-006-0004-6 (2006) (**PMC Free article**).
28. Katayama, R. et al. The new-generation selective ROS1/NTRK inhibitor DS-6051b overcomes crizotinib resistant ROS1-G2032R mutation in preclinical models. *Nat. Commun.* **10**(1), 3604. https://doi.org/10.1038/s41467-019-11496-z (2019).

29. Ahsan, H., Islam, S. U., Ahmed, M. B. & Lee, Y. S. Role of Nrf2, STAT3, and Src as molecular targets for cancer chemoprevention. *Pharmaceutics* **14**(9), 1775. https://doi.org/10.3390/pharmaceutics14091775 (2022).
30. Teli, G. et al. Medicinal chemistry perspectives on recent advances in Src kinase inhibitors as a potential target for the development of anticancer agents: biological profile, selectivity, structure-activity relationship. *Chem. Biodivers.* **20** (9), e202300515. https://doi.org/10.1002/cbdv.202300515 (2023).
31. Yu, G. T. et al. Inhibition of SRC family kinases facilitates anti-CTLA4 immunotherapy in head and neck squamous cell carcinoma. *Cell. Mol Life Sci*. **75** (22), 4223–4234. https://doi.org/10.1007/s00018-018-2863-3 (2018).
32. Gong, W. J. et al. Resistin facilitates metastasis of lung adenocarcinoma through the TLR4/Src/EGFR/PI3K/NF-κB pathway. *Cancer Sci.* **109** (8), 2391–2400. https://doi.org/10.1111/cas.13704 (2018).
33. Alcalá, S. et al. Targeting SRC kinase signaling in pancreatic cancer stem cells [published correction appears in Int. *J. Mol. Sci*. 2020 Dec 03;21(23)]. *Int. J. Mol. Sci.* **21**(20), 7437. https://doi.org/10.3390/ijms21207437 (2020).
34. Xu, S. et al. CXCR7 promotes melanoma tumorigenesis via Src kinase signaling. *Cell. Death Dis.* https://doi.org/10.1038/s41419-019-1442-3 (2019).
35. Wiese, W. et al. PI3K/Akt/mTOR signaling pathway in blood malignancies—new therapeutic possibilities. *Cancers (Basel)* **15**(21), 5297. https://doi.org/10.3390/cancers15215297 (2023).
36. Morgos, D. T. et al. Targeting PI3K/AKT/mTOR and MAPK signaling pathways in gastric cancer. *Int. J. Mol. Sci.* **25**(3), 1848. https://doi.org/10.3390/ijms25031848 (2024).
37. Mu, X. et al. Asiaticoside-nitric oxide synergistically accelerate diabetic wound healing by regulating key metabolites and SRC/STAT3 signaling. *Burns Trauma.* **13**, tkaf009. https://doi.org/10.1093/burnst/tkaf009 (2025).
38. Saridaki, Z., Souglakos, J. & Georgoulias, V. Prognostic and predictive significance of MSI in stages II/III colon cancer. *World J. Gastroenterol.* **20**(22), 6809–6814. https://doi.org/10.3748/wjg.v20.i22.6809 (2014).
39. Arredondo, J. et al. Neoadjuvant chemotherapy in locally advanced colon cancer: a systematic review. *Tech. Coloproctol* **24**(10), 1001–1015. https://doi.org/10.1007/s10151-020-02289-4 (2020) (**PMC Free article**).
40. Tian, A. et al. Triggering pyroptosis enhances the antitumor efficacy of PARP inhibitors in prostate cancer. *Cell. Oncol. (Dordr)*. **46** (6), 1855–1870. https://doi.org/10.1007/s13402-023-00860-3 (2023).
41. Jiang, M., Qi, L., Li, L. & Li, Y. The caspase-3/GSDME signal pathway as a switch between apoptosis and pyroptosis in cancer. *Cell. Death Discov*. **10** (6), 112. https://doi.org/10.1038/s41420-020-00349-0 (2020).

Acknowledgements

We would like to thank Editage (www.editage.cn) for English language editing.

Author contributions

TZ, YZ, and SZ collected the data, wrote and edited the manuscript. YW, SH and WY provided research materials and technical support. MY, TL and SD confirm the authenticity of all the raw data. DW and YX directed the project and reviewed the manuscript. All authors contributed to manuscript composition, and all authors have read and approved the final version of the manuscript.

Funding

This study was funded by the National Natural Science Foundation of China (82203157, 82273574, 82273433), Sichuan Provincial Department of Science and Technology (2024ZYD0027), Foundation of Health Commission of Chengdu (2024077), Foundation of Sichuan Medical and Health Care Promotion Institute (KY2022QN0313), Foundation of Chengdu Medical College (CYYZZ24-02, 24LHBBYY1-01, 2024bjGzn01).

Declarations

Competing interests

The authors declare no competing interests.

Ethical approval

This study was approved by the Ethics Committee of the Chengdu Medical College (approval number: 2020-15). All methods are reported in accordance with ARRIVE guidelines.

Additional information

Supplementary Information The online version contains supplementary material available at https://doi.org/10.1038/s41598-025-02901-3.

Correspondence and requests for materials should be addressed to Y.X.